

PII: S0017-9310(96)00359-6

# Modelling of frost growth and densification

R. LE GALL and J. M. GRILLOT

Groupement pour la Recherche sur les Echangeurs Thermiques, GRETh/CENG,  
17 Rue des Martyrs, 38054 Grenoble Cedex 09, France

and

C. JALLUT

Laboratoire d'Automatique et de Génie des Procédés, LAGEP—UPRES A CNRS Q 5007,  
Université Claude Bernard Lyon I—CPE Lyon, 43 bd du 11 Novembre 1918, 69622  
Villeurbanne Cedex, France

(Received 20 February 1995 and in final form 24 September 1996)

**Abstract**—A one-dimensional transient formulation is derived to predict frost growth and densification on a cold wall submitted to a moist air flow. The model is based on a local volume averaging technique that allows the computation of temperature and density distributions throughout the entire frost layer according to time. It is particularly shown that the effective vapour mass diffusivity throughout frost should reach values several times larger than the molecular diffusivity, so that the model is in agreement with experimental data. In order to represent this phenomenon, a new expression for the so-called diffusion resistance factor is proposed. Values of an adjustable parameter appearing in this expression are correlated to heat and mass transfer boundary conditions, and to the global rate of densification. Two possible interpretations of the phenomenon are proposed. © 1997 Elsevier Science Ltd.

## INTRODUCTION

Each time moist air is exposed to a cold surface whose temperature is below 0°C, frost formation occurs. Therefore, it affects numerous fields of industry working with low temperatures, including heat exchangers, aeronautics and cryogenics. Frost formation in heat exchangers (domestic and/or industrial refrigeration) must be particularly avoided because of its adverse effect upon heat transfer and pressure loss. Consecutive defrosting and ice deterioration, which increase costs, are also reasons why frost is highly undesirable.

Despite the large amount of previous work (see, for example, refs. [1, 2]) dealing with that process, there is still a considerable need for a more comprehensive and reliable method of predicting frost formation. This is mainly due to the complex tasks involved: frost formation is a non-linear, transient and coupled heat and mass problem with a moving boundary. It is also experimentally hard to investigate due to the unstable and brittle nature of the deposit.

Most of the models previously proposed (Brian *et al.* [3], and Jones and Parker [4]) for frost growth are based on the assumption that the frost density is uniform throughout the entire frost layer. The use of an average frost density helped the authors to use simplified heat and mass balances applying to the frost layer. Although it gives some appreciable results, this formulation is not physically relevant, and does not

allow the description of all of the phenomena occurring during frost growth.

Earlier, Shah [5] and Sanders [6] tried to consider spatial variations in the frost density. They failed, in part due to the complexity involved, and because they wanted to apply the model to a frost formed at very low temperatures ( $\theta_w = -196^\circ\text{C}$ ). At these cryogenic temperatures, other mechanisms, like thermal diffusion of ice particles, seem to occur.

More recently, Tao *et al.* [7–9] also developed a mathematical model that allows both spatial and temporal variations in the frost density and temperature. This model is quite similar to that proposed here, except for the treatment of the boundary conditions and the permeation period. Their work resulted from numerous and interesting previous investigations [10] held on water vapour diffusion and frost formation in porous media.

## DESCRIPTION OF THE FROST GROWTH

Hayashi *et al.* [11] considered three periods which describe the evolution of a frost layer, and are now widely accepted. From the beginning, when the clean cold plate is exposed to the ambient moist airstream, they noticed:

- the crystal growth period,
- the frost layer growth period,
- the frost layer full-growth period.

## NOMENCLATURE

$C_p$	specific heat capacity at constant pressure [J kg <sup>-1</sup> K <sup>-1</sup> ]	$\varepsilon$	volumetric fraction
$d$	reference dimension [m]	$\eta$	coordinate axis
$D_h$	hydraulic diameter [m]	$\theta$	temperature [°C]
$D_{AB}$	vapour–air binary molecular diffusivity [m <sup>2</sup> s <sup>-1</sup> ]	$\lambda$	thermal conductivity [W m <sup>-1</sup> K <sup>-1</sup> ]
$D_{\text{eff}}$	effective diffusivity [m <sup>2</sup> s <sup>-1</sup> ]	$\mu$	diffusion resistance factor
$F_{\mu}, F$	fitting parameters for the diffusion resistance factor [equations (25) and (26)]	$\nu$	kinematic viscosity [m <sup>2</sup> s <sup>-1</sup> ]
$Fo$	Fourier number ( $\alpha t/d^2$ )	$\zeta(T) = (\partial\rho_{\text{vi}}/\partial T)$	thermodynamic function [kg m <sup>-3</sup> K <sup>-1</sup> ] [equation (9)]
$h_c$	heat transfer coefficient [W m <sup>-2</sup> K <sup>-1</sup> ]	$\rho$	density [kg m <sup>-3</sup> ]
$k$	fitting parameter for the diffusion resistance factor [equation (26)]	$\tau$	tortuosity
$k_p$	mass transfer coefficient [m s <sup>-1</sup> ]	$\zeta$	parameter for the full growth period modelling [equation (21)].
$L$	latent heat [J kg <sup>-1</sup> ]	<b>Subscripts</b>	
$m$	rate of phase change for water vapour [kg m <sup>-3</sup> s <sup>-1</sup> ]	a	air
$M$	molecular weight [kg mol <sup>-1</sup> ]	c	conduction
$n_d$	water vapour mass flux [kg m <sup>-2</sup> s <sup>-1</sup> ]	s	frost surface
$p$	pressure [Pa]	sv	solid–vapour
$q$	heat flux [W m <sup>-2</sup> ]	t	total
$R$	ideal gas constant [J K <sup>-1</sup> mol <sup>-1</sup> ]	tp	triple point
$Re$	Reynolds number ( $Vd/\nu$ )	v	water vapour
$t$	time [s]	vsi	water vapour saturated over ice
$T$	temperature [K]	w	cold wall
$v$	velocity [m s <sup>-1</sup> ]	$\alpha$	ice
$V$	volume [m <sup>3</sup> ]	$\gamma$	gaseous phase (moist air)
$W$	humidity ratio [kg kg <sup>-1</sup> ]	$\infty$	bulk condition.
$x$	coordinate axis parallel to air flow.	<b>Superscripts</b>	
<b>Greek symbols</b>		0	initial time
$\alpha$	thermal diffusivity [m <sup>2</sup> s <sup>-1</sup> ]	*	dimensionless
$\beta(T)$	thermodynamic function [kg m <sup>-1</sup> K <sup>-1</sup> s <sup>-1</sup> ] [equations (13) and (14)]	$\bar{\cdot}$	spatial-averaged
		$\sim$	time-averaged
		$\dot{\cdot}$	time-derivative.
		<b>Other</b>	
		$\nabla$	gradient following $\eta$ -direction ( $\partial/\partial\eta$ ) [m <sup>-1</sup> ].

The first and rather short period is characterized by the condensation and subsequent freezing of small water droplets. Next, frost crystals are generated on these ice *nuclei*, and grow in a vertical direction at about the same rate. Although there exist some attempts to describe this period more precisely [8, 12], it is believed that the modelling of the crystal growth is not really relevant to the present problem, and leads to needless complications of the formulation: it will be involved here only in the choice of the initial properties of the frost layer.

The present model applies to the following periods, which represent most of the frost layer evolution. During these two periods, the frost layer is characterized by a more uniform aspect due to the branching and interconnecting of the ice crystals. The frost layer becomes like an homogeneous porous material made

of a solid ice matrix and pores filled with moist air. The mass transfer towards the frost layer leads to the growth and densification of the porous deposit.

The frost layer full-growth period arises when the surface temperature becomes equal to the water triple-point temperature ( $T_s = T_{\text{tp}}$ ) due to increased frost thermal resistance. Water vapour condensing at the top of the frost layer forms a liquid film that soaks into the frost layer, and freezes in the colder areas towards the cold wall. Then, a cyclic process of melting, freezing and growth occurs until thermal equilibrium of the entire frost layer is reached.

#### Frost growth modelling

**Basic assumptions.** The present model is based on the following assumptions: (a) one-dimensional transport processes (like frost formation on a flat plate

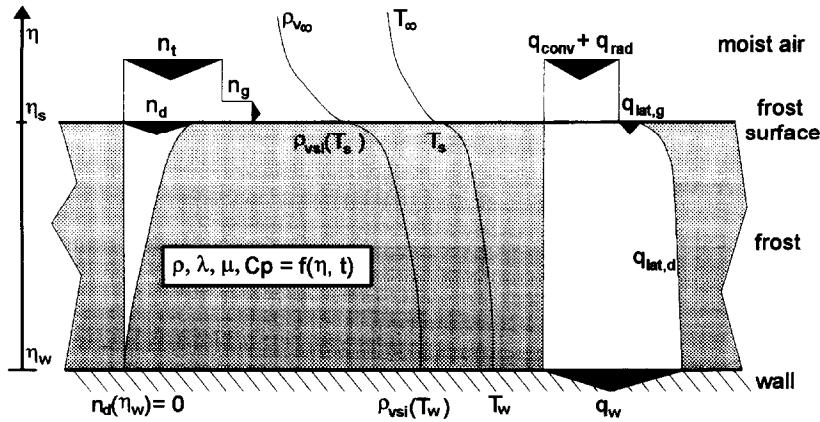


Fig. 1. Coupled heat and mass transfer during frost formation.

or a tube) are assumed; (b) perfect gas law and local thermodynamic equilibrium conditions prevail [1, 13]; (c) the total gas phase pressure  $p_t$  is constant throughout the porous frost layer, and equal to the normal atmospheric pressure; (d) convection and radiation effects are negligible within the frost structure [13]; (e) Soret and Dufour effects are negligible; (f) resolution begins at time  $t^0$ , when the frost layer can be considered as a uniform porous layer of width  $\eta_s^0$  and average density  $\bar{\rho}_0$ ; and (g) temperature variations of moist air and ice properties are neglected.

The frost layer is a porous medium considered as pseudo-homogeneous, where heat and mass transfer are described, respectively, by Fourier's and Fick's laws. Due to the thermodynamic equilibrium conditions prevailing throughout the frost layer, these two transport phenomena are coupled (Fig. 1)

The 'local volume averaging technique' described in refs. [14, 15] may then be used. Here it consists in considering an elementary control volume  $V$ , where both ice ( $V_a$ ) and moist air ( $V_v$ ) coexist (Fig. 2). The ice and moist air volumetric fractions are then simply related to the control volume  $V$  by

$$\varepsilon_x = V_x/V \quad \text{and} \quad \varepsilon_y = V_y/V \quad (1)$$

with

$$\varepsilon_x + \varepsilon_y = 1 \quad \text{and} \quad \left(\frac{\partial \varepsilon_x}{\partial t}\right) = -\left(\frac{\partial \varepsilon_y}{\partial t}\right). \quad (2)$$

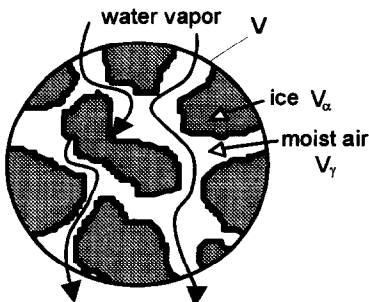


Fig. 2. Elementary control volume.

The equivalent thermo-physical properties of this medium are defined as follows:

$$\rho = \varepsilon_x \rho_x + \varepsilon_y (\rho_a + \rho_v) \quad (3)$$

$$\rho C_p(\varepsilon_x, T) = \varepsilon_x \rho_x C_{p_x}(T) + \varepsilon_y (\rho_a C_{p_a} + \rho_v C_{p_v}). \quad (4)$$

Consequently, the elementary control volume is simply characterized by its temperature  $T$  and its volumetric ice fraction  $\varepsilon_x$ .

The air and water vapour densities are derived from a perfect gas law and thermodynamic equilibrium assumption:

$$\rho_v = \rho_{vsi}(T) = \frac{M_v}{RT} p_{vsi}(T)$$

$$\text{and} \quad \rho_a = \frac{M_a}{RT} [p_t - p_{vsi}(T)]. \quad (5)$$

The physical properties of ice, water vapor and air are found in Table 1.

*Balance equations.* If we define  $\dot{m}$  as the volumetric rate of phase change, the water balance over the ice phase is

$$\dot{m} = -\rho_x \left(\frac{\partial \varepsilon_x}{\partial t}\right). \quad (6)$$

Positive values of  $\dot{m}$  correspond to sublimation of the ice matrix, whereas negative values are related to

Table 1. Physical properties (from ref. [1])

$p_{vsi}$	[Pa]	$\exp\left(\frac{22.376 \times \theta}{271.68 + \theta} + 6.4146\right)$
$C_{p_a}$	[J kg <sup>-1</sup> K <sup>-1</sup> ]	1006
$C_{p_v}$	[J kg <sup>-1</sup> K <sup>-1</sup> ]	1826.6
$C_{p_x}(\theta)$	[J kg <sup>-1</sup> K <sup>-1</sup> ]	$2109 + 3.66\theta$
$L_{sv}$	[J kg <sup>-1</sup> ]	$2834.5 \times 10^3$
$\rho_x$	[kg m <sup>-3</sup> ]	917
$D_{AB}$	[m <sup>2</sup> s <sup>-1</sup> ]	$1.451 \times 10^{-4} \frac{T^{1.72}}{P_t}$

condensation of the water vapour into ice (ablimation).

Thereafter, the water and energy balances over the equivalent pseudo-homogeneous medium are:

$$\dot{m} - \left( \frac{\partial \rho_v \varepsilon_x}{\partial t} \right) = \nabla n_d \quad (7)$$

$$\rho C_p \left( \frac{\partial T}{\partial t} \right) + L_{sv} \dot{m} = \nabla (\lambda_c \nabla T) \quad (8)$$

where  $n_d$  is the water vapour mass flux and  $\lambda_c \nabla T$  is the conductive thermal flux (see the Appendix). The volumetric rate of phase change ( $\dot{m}$ ), which appears in both equations, represents the coupling term between heat and mass transfer. Each term of equations (7) and (8) can be expressed as a function of the two independent variables  $\varepsilon_x$  and  $T$ .

By combining equations (6)–(8), one obtains a coupled system of non-linear partial derivative equations, of which  $\varepsilon_x$  and  $T$  are solutions:

$$\begin{cases} [\xi(T)(1 - \varepsilon_x)] \left( \frac{\partial T}{\partial t} \right) + [\rho_x - \rho_{vsi}(T)] \left( \frac{\partial \varepsilon_x}{\partial t} \right) = \nabla n_d \\ [\rho C_p(\varepsilon_x, T)] \left( \frac{\partial T}{\partial t} \right) - (L_{sv} \rho_x) \left( \frac{\partial \varepsilon_x}{\partial t} \right) = \nabla [\lambda_c(\varepsilon_x, T) \nabla T] \end{cases} \quad (9)$$

This system is solved using a common finite difference method [16] with fully implicit time resolution applied to the entire discretized frost layer. Due to the non-linearity of the equations, a proper iteration scheme, including under-relaxation, is used.

At each time step, the grid spacing is modified to fit the new frost thickness. In this way, the spatial grid resolution is fixed and will not change with frost growth. An intermediate value of 20 grid points is chosen to obtain a compromise between the accuracy and computation time.

The time steps are low enough (especially at the beginning of the resolution) to ensure stability and to minimize error due to the interpolations. More details about numerical and computational procedures can be found in ref. [1].

*Water vapour transport.* The effective water vapour transport occurring in frost still remains the most complex phenomenon to investigate. This is due to the lack of reliable experimental data about effective water transport in such a porous medium involving phase changes. In the case of frost, the solid matrix (ice phase) is not fixed as in common porous media, but continuously evolves during the growing of the frost layer.

There is a great agreement in the literature (see, for example, refs. [6, 17]) on the fact that the water transport through a porous medium is mainly due to Fickian diffusion caused by the vapour partial pressure gradient:

$$n_d = -D_{\text{eff}} \left( \frac{M_v}{RT} \right) \left( \frac{p_t}{p_t - p_v} \right) \nabla p_v. \quad (10)$$

According to the local thermodynamic equilibrium hypothesis, and in combination with the perfect gas law and Clausius–Clapeyron expression,  $n_d$  may also be related to the temperature gradient:

$$n_d = -D_{\text{eff}} \left( \frac{M_v^2 L_{sv}}{R^2 T^3} \right) \left[ \frac{p_t p_{vsi}(T)}{p_t - p_{vsi}(T)} \right] \nabla T. \quad (11)$$

The effective diffusivity  $D_{\text{eff}}$  accounts for a combination of the following complex physical mechanisms involved in the evolution of the frost porous medium:

- ordinary diffusion,
- decreasing of the effective cross-sectional area,
- tortuosity of the porous medium,
- phase transitions (condensation and/or sublimation),
- metamorphism within the frost structure,
- variations of gaseous pressure within the small pores, ...

The derivation of a complete analytical expression of the effective diffusivity  $D_{\text{eff}}$  is then a very complex task, and needs more experimental and theoretical research. Nevertheless, in order to be consistent with other work dealing with gaseous diffusion through porous media,  $D_{\text{eff}}$  is simply expressed as a function of the molecular water vapour diffusivity in moist air ( $D_{AB}$ ):

$$D_{\text{eff}} = \mu D_{AB} \quad (12)$$

where  $D_{AB}$  is given by an empirical expression [1] (see Table 1 for  $D_{AB}$  calculation), and  $\mu$  is the diffusion resistance factor (usually less than 1).

Finally, by defining  $\beta(T)$  as a function only of the temperature, the expression for the water vapour mass flux reduces to

$$n_d = -\mu(\varepsilon_x) \beta(T) \nabla T \quad (13)$$

with

$$\beta(T) = D_{AB} \left( \frac{M_v^2 L_{sv}}{R^2 T^3} \right) \left[ \frac{p_t p_{vsi}(T)}{p_t - p_{vsi}(T)} \right]. \quad (14)$$

This formulation characterizes the water vapour mass flux in terms of a structure function  $[\mu(\varepsilon_x)]$ , a temperature function  $[\beta(T)]$ , and the local temperature gradient.

*Boundary conditions.* The boundary conditions are related to the heat and mass transfer prevailing at the wall and the frost surface (Fig. 1).

The wall conditions ( $\eta = \eta_w$ ) are straightforward:

$$\begin{cases} T(\eta_w) = T_w \\ n_d(\eta_w) = 0 \end{cases} \quad (15)$$

The total mass flux delivered by convection at the frost surface is a function of the frost surface temperature:

$$n_t = k_p[\rho_{v\infty} - \rho_{vst}(T_s)]. \quad (16)$$

The water vapour mass flux diffusing through the frost surface  $[n_d(\eta_s)]$  is given by

$$n_d(\eta_s) = \mu(\eta_s)\beta(T_s)\nabla T_s. \quad (17)$$

In the case of frost growth,  $n_t$  exceeds  $n_d(\eta_s)$ , so that some water will condense at the top, thus contributing to the subsequent growth of the frost layer according to

$$\rho(\eta_s)\left(\frac{\partial\eta_s}{\partial t}\right) = n_t - n_d(\eta_s) \quad (18)$$

where  $\rho(\eta_s)$  is the frost surface density.

The heat balance at the interface leads to the following condition:

$$\lambda_c\nabla T_s = h_c(T_\infty - T_s) + L_{sv}[n_t - n_d(\eta_s)]. \quad (19)$$

The convective heat and mass transfer coefficients are given by classical correlations [18]. The transfer characteristics might also be derived from a Chilton–Colburn analogy (see, for example, refs. [6, 19]).

Some direct measurements of the heat and mass transfer characteristics also provide proper boundary conditions for the resolution of equations (9).

In their model, Tao *et al.* [8] postulated additional constraints, such as a zero gradient in the ice fraction at both boundaries (wall and surface) of the frost layer. It seems that there is no need for additional constraints, and that the aforementioned heat and mass transfer conditions are sufficient for the resolution of system (9). They also pointed out [9] a possible difference between the surface effective diffusivity acting at the frost–air interface and the ‘volumetric’ effective diffusivity as described by equation (11); this will not be considered here.

#### Initial and final time resolution

*Initial conditions and crystal growth period.* The resolution begins at time  $t^0$ , for which the frost layer is considered as a uniform porous layer of width  $\eta_s^0$  and average density  $\bar{\rho}^0$ . To extrapolate the model to times corresponding to the crystal growth period, it is desirable to choose the lowest possible values of  $\eta_s^0$  and  $\bar{\rho}^0$ , when frost deposition is just occurring: the values  $\eta_s^0 = 0.1$  mm and  $\bar{\rho}^0 = 25$  kg m<sup>-3</sup> seem to be convenient from sensitivity calculations carried out on the model (see ref. [1]).

In order to take into account the initial period when frost growth is comparatively fast, the growth density  $\rho(\eta_s)$  is taken as

$$\rho(\eta_s) = \bar{\rho}^0 \quad \text{for } t \leq t^0 + 60 \quad \text{or} \quad \eta_s \leq 0.5 \text{ mm}. \quad (20)$$

During this initial period, the rapid frost growth will correspond to the crystal growth described in ref. [11].

*Frost layer full-growth period.* When the frost layer enters the full-growth period (i.e. when the frost surface temperature reaches the water triple-point tem-

perature), some liquid water soaks towards the surface. This process, called permeation, has been studied by Aoki *et al.* [20]; the infiltration of liquid in the porous layer is due to capillary and/or gravity effects. During this period, the frost layer undergoes a cycle of thinning and densification due to the melting and subsequent formation on an icy sublayer at the top of the deposit. In this part of the frost layer, water transportation is mainly due to permeation, whereas diffusion of water vapour is still going on throughout the rest of the frost layer.

In order to take into account this phenomenon, when some control volumes on top of the frost layer reach the melting-point ( $T \geq T_{tp}$ ) (Fig. 3), the corresponding water mass is simply redistributed to the underlying elements as follows:

$$\varepsilon'_x = \varepsilon_x + \zeta(1 - \varepsilon_x) \quad \varepsilon'_x \geq \varepsilon_x \quad \text{and} \quad 0 \leq \zeta \leq 1. \quad (21)$$

The ice fractions  $\varepsilon_x$  of the control volumes concerned are corrected according to their available porosity until the liquid film is totally consumed. The volumetric fraction  $\zeta$  allows a choice between a more or less important infiltration depth for the liquid film.

No sensitivity study was performed for  $\zeta$ , the permeation phenomenon being beyond the scope of the present study. For the sake of generality, a mean value of  $\zeta = 0.5$  has been chosen.

As the time-scale of permeation is negligible compared to that of water vapour diffusion, this process is considered to act as soon as the water triple-point temperature is reached. The heat and mass boundary conditions, as well as the frost surface temperature condition ( $T_s \leq T_{tp}$ ), applying to the frost layer are still considered during this process.

## RESULTS AND DISCUSSION: DIFFUSION RESISTANCE FACTOR ESTIMATION

As already pointed out, the main problem concerns the correct evaluation of the water vapour diffusion resistance  $\mu$  [see equation (12)], for which no direct measurements are available.

The most commonly used expressions for  $\mu$  are simply related to the porous medium porosity (or ice phase volumetric fraction):

$$\mu \equiv \mu(\varepsilon_x). \quad (22)$$

Simple empirical expressions, issued from measurements upon a fixed bed of glass particles, can be found elsewhere, and are widely used for lumped frost formation models (see, for example, refs. [3, 12]):

$$\mu = (1 - \varepsilon_x)/\tau \quad 1.1 \leq \tau \leq 1.3 \quad (23)$$

where  $\tau$  is the tortuosity of the porous medium.

Another expression of  $\mu$  is that of Auracher [21], who did theoretical studies on frost structure models and some careful measurements of water vapour diffusion during frosting in capillary tubes:

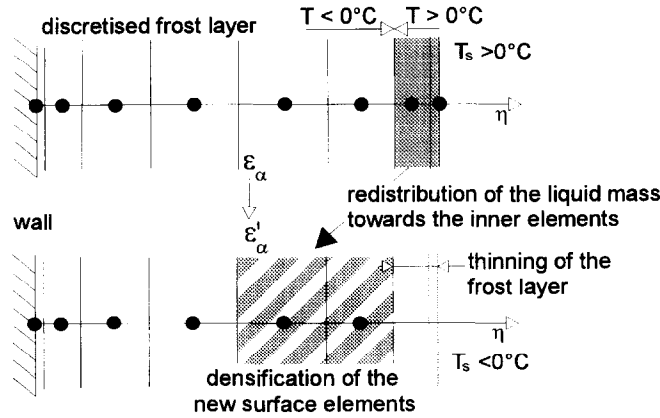


Fig. 3. Adaptation of the model to the permeation process.

$$\mu = \frac{1 - \varepsilon_x}{1 - C_0 \varepsilon_x} \quad \text{with } C_0 = 0.58. \quad (24)$$

Unfortunately, the range of boundary conditions covered by this study is very limited, and cannot apply to all frosting conditions.

The above two expressions [equations (23) and (24)] always lead to effective diffusivities lower than the molecular one ( $\mu \leq 1$ ). Nevertheless, other investigations (Yosida [22]) carried out on water vapour diffusion through snow (which is very similar to frost) show a great discrepancy, and result in a diffusion resistance factor  $\mu$  much greater than 1 (up to 10). The author pointed out that, in the particular case of frost (or snow), the diffusing substance (water vapour) is the same as the solid matrix (ice). Thus, it can go ‘through’ the ice crystals by simply condensing on one side, releasing its latent heat, thus allowing some more ice to sublimate on the other side (Fig. 2). This process, called ‘hand-to-hand’ diffusion, could justify the large values proposed for the water vapour effective diffusivity.

Tao *et al.* [8] also obtained effective diffusivities several times larger (up to 7) than the molecular one. In order to take into account this result, they defined a parameter  $F$  related to  $\mu$  by

$$\mu = (1 + F)(1 - \varepsilon_x). \quad (25)$$

Depending on the  $F$  value,  $\mu$  may be greater than 1.

It appears to be very difficult to choose among all these simple formulations that are not really in

agreement. It is believed that the frost diffusion resistance factor is a much more complex function that involves structural effects (ice fraction  $\varepsilon_x$ ) as well as other ambient conditions prevailing in the frost layer.

Expression (25), derived from Auracher’s works [13, 21] was used first; the results obtained were not really satisfying, and did not always fit the experimental data. Most of the time, the water vapour transport seemed too low to ensure correct estimations of the frost thickness and average density. The diffusion resistance factor  $\mu$  given by Auracher was thus artificially increased by adding an arbitrary second term, a function of the ice volumetric fraction  $\varepsilon_x$  and the two parameters  $k$  and  $F_\mu$ :

$$\mu(\varepsilon_x, F_\mu) = \frac{1 - \varepsilon_x}{1 - C_0 \varepsilon_x} + F_\mu k \varepsilon_x (1 - \varepsilon_x)^k \quad \text{with } \begin{cases} C_0 = 0.58 \\ k = 10 \end{cases} \quad (26)$$

The first exponent ( $k$ ) allows the increase to be distributed throughout the whole range of the ice fraction  $\varepsilon_x$  [Fig. 4(a)]; it is fixed at 10 to ensure a maximum value in the area of low  $\varepsilon_x$  (corresponding to high porosities). The parameter  $F_\mu$  affects the intensity of the correction. Positive values of  $F_\mu$  lead to an effective diffusivity that can be greater than the molecular one ( $\mu > 1$ ) [Fig. 4(b)]. Formulation (26) always fits the two limiting conditions [ $\mu(\varepsilon_x = 0) = 1$  and  $\mu(\varepsilon_x = 1) = 0$ ] which apply for water vapour diffusion

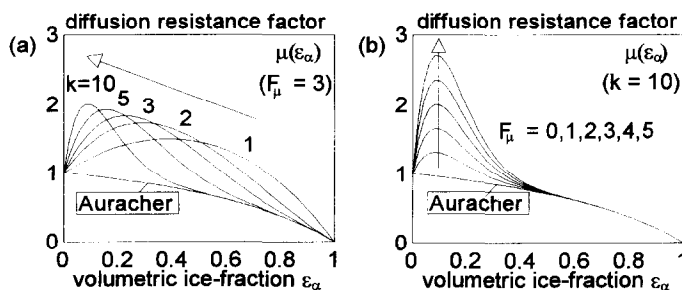


Fig. 4. (a) Effect of  $k$  on  $\mu(\varepsilon_x)$ ; (b) effect of  $F_\mu$  on  $\mu(\varepsilon_x)$ .

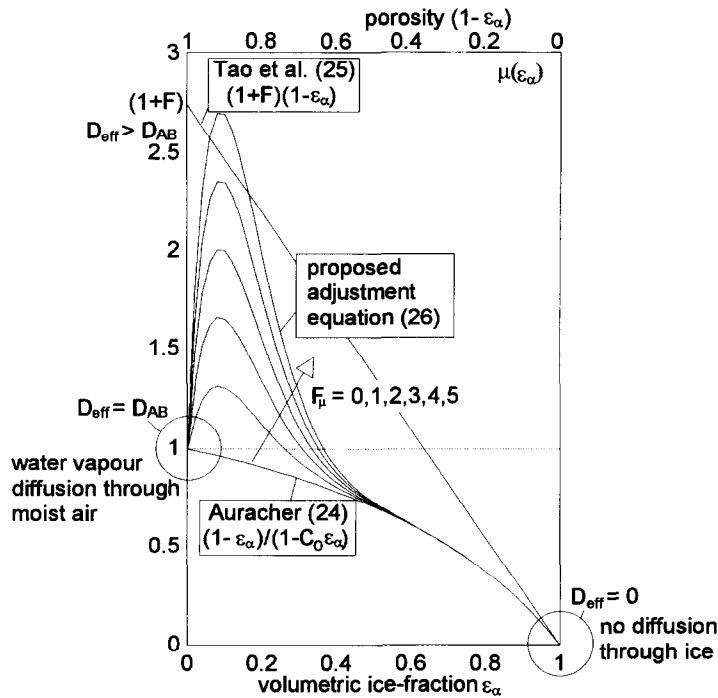


Fig. 5. Modelling of the diffusion resistance factor  $\mu(\epsilon_\alpha)$ .

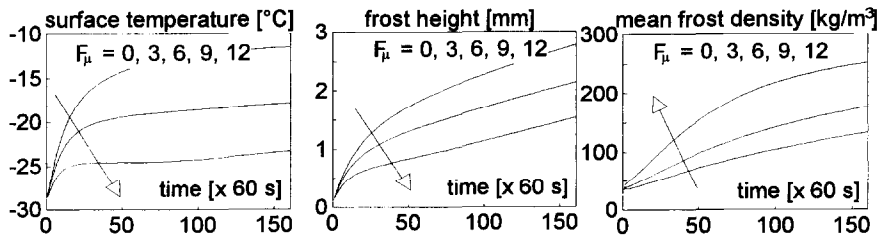


Fig. 6. Sensitivity to the diffusion resistance factor  $\mu(\epsilon_\alpha)$  ( $x = 0.5\text{m}$ ,  $W_x = 0.004\text{ kg kg}^{-1}$ ,  $T_x = 15^\circ\text{C}$ ,  $T_w = -30^\circ\text{C}$ ,  $v_{x_0} = 3.6\text{ m s}^{-1}$ ).

through, respectively, air and ice: it appears to be a compromise between Auracher’s expression (24) and the Tao *et al.* ones (25) (Fig. 5)

Figure 6 shows that the model results are strongly sensitive to  $F_\mu$  (and, thus, to the diffusion factor  $\mu$ ): higher values of  $F_\mu$  correspond to thinner and denser frost layers. It is, therefore, proposed that some variations in this factor  $\mu$  could be responsible for the great discrepancy observed between the experimental and theoretical data. As pointed out by Tao and Besant [9], these variations should be related to the different boundary conditions applied to the frost layer.

*F<sub>μ</sub> estimation from the experimental results*

In order to validate the proposed model, an experimental set-up was built whose main characteristics were:

- the frost grew on the external surface of a stainless steel tube (1.8 m length, 0.02 m outer diameter) from moist air,
- the moist air flowed through an annular section

between the inner tube and a plexiglass tube (0.037 m inner diameter). The inlet temperature and moisture of the air flux were controlled as well as its rate of flow,

- the inner tube was cooled by a liquid R11 flow.

Global measurements (inlet and outlet air temperature, and moisture) as well as local ones (frost surface temperature and thickness) were performed according to the air flow, temperature, and moisture and inner-tube temperature. All of the details concerning this pilot set-up are available in ref. [1].

The most useful information retained to estimate  $F_\mu$  was the frost surface temperature, which was continuously measured using an infrared radiometer. For each set of experimental conditions,  $F_\mu$  was estimated by trial and error. Figure 7 shows two examples of the good results obtained with  $0 < F_\mu < 1.5$ . Nevertheless, it is generally difficult to get a single satisfying value of  $F_\mu$  for the whole test duration. This is mainly due to the confinement ( $D_h \leq 0.017\text{ m}$ ) of the annular test section, which leads to important variations in the boundary conditions during frost growth (all tests

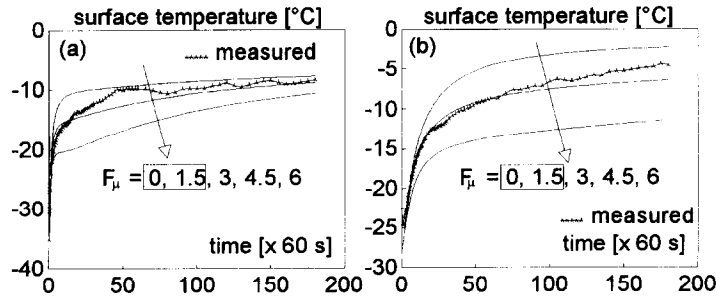


Fig. 7. Adjustments of the model with our experimental results. (a)  $x = 0.5$  m,  $W_s = 0.004$  kg kg<sup>-1</sup>,  $T_s = 15^\circ\text{C}$ ,  $T_w = -40^\circ\text{C}$ ,  $v_s^0 = 18.2$  m s<sup>-1</sup>; (b)  $x = 0.5$  m,  $W_s = 0.006$  kg kg<sup>-1</sup>,  $T_s = 15^\circ\text{C}$ ,  $T_w = -30^\circ\text{C}$ ,  $v_s^0 = 3.6$  m s<sup>-1</sup>.

were performed at a constant rate of flow). A correct adjustment of the model would have required a varying  $F_\mu$  corresponding to the varying conditions.

*F<sub>μ</sub> estimation from literature data*

Considering this difficulty, it was decided to use the Mao *et al.* [24, 25] empirical correlations. They measured the boundary conditions as well as the main characteristics of a frost layer growing on a cold flat plate submitted to a forced circulation of moist air. More than 90 tests were done for the whole range of parameters defined in Table 2. All of their results are expressed in terms of correlations for the dimensionless independent variables defined as: a position ratio  $x^* = x/D_h$ , the humidity ratio  $W_s$ , a reduced temperature,  $T^*[(T_{ip} - T_w)/(T_s - T_w)]$ , the Reynolds number  $Re_{Dh}$ , and the Fourier number  $Fo_{Dh}$ . The reference dimension of the rectangular flow channel is  $D_h = 0.0375$  m (twice the present value); variations due to frost growth are then neglected. Two sets of empirical correlations are obtained, corresponding, respectively, to turbulent [24] and laminar [25] flow conditions. The total heat flux delivered to the wall is directly measured by a heat fluxmeter.

The Mao *et al.* correlations [24, 25] were extrapolated towards initial times ( $t^0 = 60$  s) to obtain some proper initial conditions ( $\eta_s^0$  and  $\bar{p}^0$ ) applying for the resolution. Unfortunately, Mao *et al.* did not measure the actual frost surface temperature, and assumed that it was always equal to  $T_{ip}$  ( $\equiv 0^\circ\text{C}$ ). It could not, therefore, be used for the present adjustments (it would

be extremely useful to improve the validation of the permeation process).

The  $F_\mu$  adjustments were then performed to fit the present model to the frost layer height and mean density correlations obtained by the authors (Fig. 8). About 50 adjustment tests of this kind have been performed to cover the whole range of parameters (including turbulent and laminar flow conditions) described in Table 2. The resulting  $F_\mu$  values ranged from about  $-2$  to  $20$ , which corresponds to a maximum effective water vapour diffusion coefficient up to 8 times the molecular one. It was then possible to establish two correlations between the  $F_\mu$  values and the corresponding boundary conditions.

First, the dimensionless independent variables isolated by Mao *et al.* [24, 25] for their empirical correlations were used. The following regression was obtained:

$$(F_\mu + 5) = 4.35x^{*0.36} W_s^{1.59} T^{* - 0.93} Re_{Dh}^{0.86} \tag{27}$$

$Fo_{Dh}$  was not used for this correlation because it was considered that the time-evolution of the different boundary conditions during the duration of the frost tests is not significant in this case ( $D_h = 0.0375$  m). The agreement between predicted values and those resulting from trial-and-error adjustments [Fig. 9(a)] is quite satisfactory.

Some new independent variables more directly related to the boundary conditions applied to the frost layer have also been isolated. These are  $q_w$  and  $n_s$ , the

Table 2. Range of parameters investigated by Mao *et al.* [24, 25]

Laminar flow		Turbulent flow	
$1.33 < x^* < 14.13$	$0.05 < x < 0.53$ m	$1.33 < x^* < 14.13$	$0.05 < x < 0.53$ m
$0.004 < W_s < 0.007$ kg kg <sup>-1</sup>		$0.004 < W_s < 0.01$ kg kg <sup>-1</sup>	
$0.24 < T^* < 0.51$	$20 < T_s < 23^\circ\text{C}$ $-15 < T_w < -5^\circ\text{C}$	$0.24 < T^* < 0.51$	$15 < T_s < 23^\circ\text{C}$ $-15 < T_w < -5^\circ\text{C}$
$1000 < Re_{Dh} < 2100$	$0.41 < V_x < 0.86$ m s <sup>-1</sup>	$3000 < Re_{Dh} < 7000$	$1.15 < V_x < 2.67$ m s <sup>-1</sup>
$28 < Fo_{Dh} < 165$	$35 < t < 210$ min	$13 < Fo_{Dh} < 104$	$15 < t < 130$ min



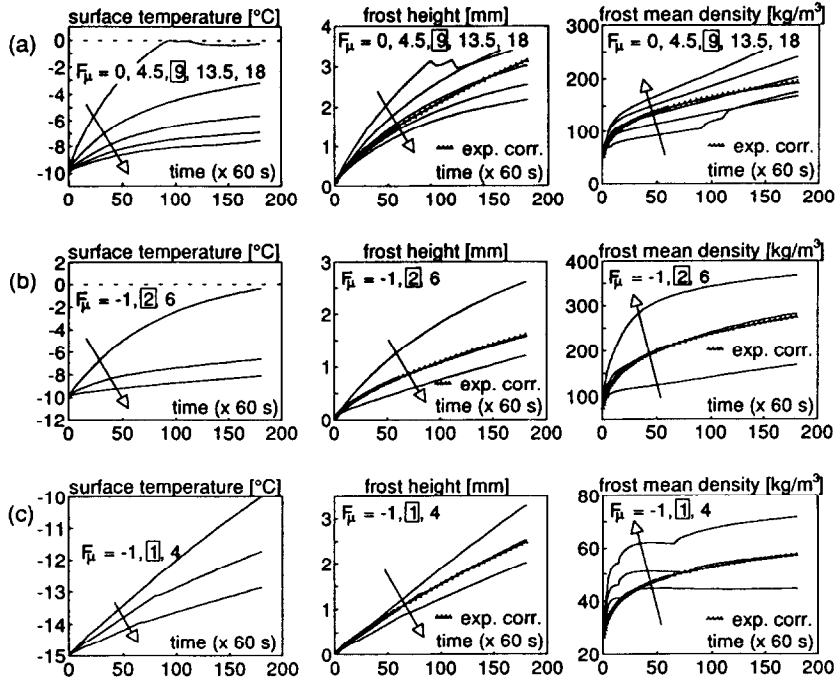


Fig. 8. Adjustments of the model with the experimental correlations obtained by Mao *et al.*: (a)  $x = 0.5$  m,  $W_x = 0.006$  kg kg<sup>-1</sup>,  $T_\infty = 20^\circ\text{C}$ ,  $T_w = -10^\circ\text{C}$ ,  $v_\infty = 3$  m s<sup>-1</sup> (turbulent flow); (b)  $x = 0.2$  m,  $W_x = 0.004$  kg kg<sup>-1</sup>,  $T_\infty = 22^\circ\text{C}$ ,  $T_w = -10^\circ\text{C}$ ,  $v_\infty = 3$  m s<sup>-1</sup> (turbulent flow); (c)  $x = 0.5$  m,  $W_x = 0.007$  kg kg<sup>-1</sup>,  $T_\infty = 20^\circ\text{C}$ ,  $T_w = -15^\circ\text{C}$ ,  $v_\infty = 0.4$  m s<sup>-1</sup> (laminar flow).

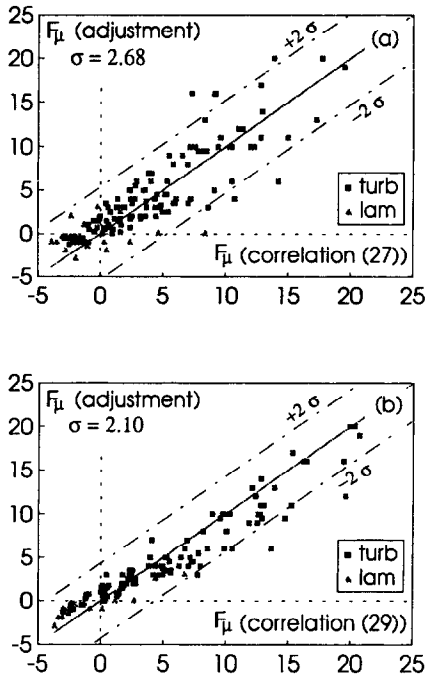


Fig. 9. Comparison of predicted and obtained values of  $F_\mu$ .

heat and mass boundary fluxes, and the global rate of densification ( $\dot{\bar{\rho}}$  [kg m<sup>-3</sup> s<sup>-1</sup>]) of the entire frost layer defined as

$$\dot{\bar{\rho}} = \frac{\partial \bar{\rho}}{\partial t} = \frac{\partial \bar{\rho}}{\partial F_{O_{Dh}}} \frac{\partial F_{O_{Dh}}}{\partial t} = \frac{\partial \bar{\rho}}{\partial F_{O_{Dh}}} (\alpha_a / D_h^2). \quad (28)$$

These parameters being slightly time-dependent, their mean time values ( $\bar{q}_w, \bar{n}_t, \bar{\rho}$ ) obtained for  $\bar{t} = 3600$  s and  $\bar{F}_{O_{Dh}} = 50$  were used. The second correlation obtained for  $F_\mu$  is then

$$(F_\mu + 5) = 8.52 \times 10^{15} \bar{q}_w^{-1.56} \bar{n}_t^{1.76} \bar{\rho}^{0.25} \quad (29)$$

with

$$\begin{cases} 50 < \bar{q}_w < 600 \\ 1.1 \times 10^{-7} < \bar{n}_t < 4.2 \times 10^{-6} \\ 8.1 \times 10^{-5} < \bar{\rho} < 1.0 \times 10^{-3} \end{cases}$$

This expression leads to a better agreement [Fig. 9(b)], although only three independent variables were used. One can especially notice that equation (29) does not depend on the parameter  $x^*$ . The dependence of  $F_\mu$  on  $x^*$  is inevitably indirect because of the boundary condition variations along the frost layer. Correlations (27) and (29) also confirm that, for the whole range of boundary conditions investigated, the realized adjustments are coherent even for the highest values ( $F_\mu \geq 10$ ) reached during the tests. This is especially noticeable as it is known that two different sets of empirical correlations covering turbulent and laminar flow conditions were used.

Accordingly, there seems to be one (or more) underlying physical mechanism(s) that could explain the increased effective diffusivity used to obtain the good agreement between the described model and the experimental data. As shown in equation (29), this mechanism should be expressed in terms of heat and mass

boundary conditions ( $q_w$  and  $n_i$ ) as well as the frost layer global rate of densification ( $\bar{\rho}$ ). No other simple environmental conditions (like  $T_w$ ,  $T_a$ , ...) could be isolated to substantially improve the above correlation.

*Possible physical explanations of the high effective water transport*

As mentioned before, it became hard to speak about common diffusion in view of the high values reached for the effective water transport. Therefore, some other physical mechanisms that could be responsible for this high observed mass transfer were investigated. Considering the literature and the results obtained, two hypotheses are proposed.

Water vapour transport through the frost is accompanied by a local consumption of the water vapour due to the phase transition in progress during frost densification. The frost layer global rate of densification  $\bar{\rho}$  [analogous to the local volumetric rate of phase change ( $-\dot{m}$ )] is then a measure of the kinetics of this transition. Hence, the change of phase occurring throughout the frost layer will act as a 'pumping' force that will promote the mass transfer mechanism: this is highly comparable to the acceleration factor introduced to describe gas-liquid absorption with chemical reaction (see, for example, ref. [26]). The above statements are supported by the fact that  $\bar{\rho}$  is directly involved (with an exponent of 0.25) in the proposed correlation (29).

Another possible explanation could result from the extreme fragility of the frost porous medium. High effective mass transfer would, in fact, be caused by displacement of some ice crystals towards the cold wall. This transfer could be due to thermophoresis acting on small ice *nuclei* (see ref. [5]), dissociation of some dendritic crystal (frost metamorphism), or more simply, a modification of the shear stress caused by the air flow along the frost layer. The great sensitivity to boundary conditions [see correlations (27) and (29)] would then be explained by mechanical and structural differences of the frost medium related to those ambient conditions. High values of  $n_i$  and  $\bar{\rho}$ , and low values of  $q_w$ , might correspond to a more fragile first structure, which will be more easily subjected to local modifications or rearrangements of the frost crystals. Moreover, it seems reasonable that those 'crammings' of the frost structure are concentrated in the low ice fraction range (high porosities), as can be seen in Fig. 5 [this was one of the most serious arguments for the choice of the  $k$  exponent introduced in expression (26)].

#### SUMMARY AND CONCLUSION

A complete and physical model of the frost layer growth and densification is presented. The achievement of the present formulation requires a good knowledge of the frost transport properties applying for, respectively, heat conduction and water diffusion.

Unfortunately, there appear to be great uncertainties about effective mass transport occurring in the frost layer. The effective water vapour transport resulting from adjustments between the model and some experimental works showed important deviations from the common Fick's diffusion. These deviations (mainly augmentation) are correlated with the heat and mass boundary conditions ( $q_w$  and  $n_i$ ) applied to the porous deposit as well as the internal global rate of densification ( $\bar{\rho}$ ). This tends to prove that some other physical mechanisms acting in conjunction with simple diffusion could be involved in the high water vapour transport prevailing in the frost layer; their identifications and characterizations will ask for more experimental and theoretical research.

*Acknowledgements*—This work was financially supported by the two French agencies ADEME (Agence de l'Environnement et de la Maitrise de l'Energie) and GRETh (Groupement de Recherche sur les Echangeurs Thermiques) which are gratefully acknowledged.

#### REFERENCES

1. Le Gall, R., Experimental study and modelling of frost formation in heat exchangers, Ph.D. thesis (in French), Institut National Polytechnique de Grenoble, Grenoble, 1994.
2. Padki, M. M., Sherif, S. A. and Nelson, R. M., A simple method for modeling the frost formation phenomenon in different geometries. *ASHRAE Transactions*, 1989, **95**, 1127–1137.
3. Brian, P. L. T., Reid, R. C. and Shah, Y. T., Frost deposition on cold surfaces. *Industrial Engineering Chemistry Fundamentals*, 1970, **9**, 375–380.
4. Jones, B. W. and Parker, J. D., Frost formation with varying environmental parameters. *Journal of Heat Transfer* 1975, 255–259.
5. Shah, Y. T., Theory of frost formation. Ph.D. thesis, Massachusetts Institute of Technology, Cambridge, MA, 1970.
6. Sanders, C. T., Frost formation: the influence of frost formation and defrosting on the performance of air coolers. Ph.D. thesis, Delft University of Technology, Delft, 1974.
7. Tao, Y. X. and Besant, R. W., Prediction of spatial and temporal distribution of frost growth on a flat plate under forced convection. *Fundamentals of Heat Transfer in Porous Media*, 1992, ASME HTD-Vol. 193, 131–139.
8. Tao, Y. X., Besant, R. W. and Rezkallah, K. S., A mathematical model for predicting the densification and growth of frost on a flat plate. *International Journal of Heat and Mass Transfer*, 1993, **36**, 353–363.
9. Tao, Y. X. and Besant, R. W., Prediction of spatial and temporal distribution of frost growth on a flat plate under forced convection. *Journal of Heat Transfer*, 1993, **115**, 278–281.
10. Tao, Y. X., Besant, R. W. and Rezkallah, K. S., Unsteady heat and mass transfer with phase changes in an insulation slab: frosting effects. *International Journal of Heat and Mass Transfer*, 1991, **34**, 1593–1603.
11. Hayashi, Y., Aoki, A., Adachi, S. and Hori, K., Study of frost properties correlating with frost formation types. *Journal of Heat Transfer*, 1977, **99**, 239–245.
12. Seki, N., Fukusako, S., Matsuo, K. and Uemura, S., Incipient phenomena of frost formation. *Bulletin of the JSME*, 1984, **27**, (233), 2476–2482.
13. Auracher, H., Effective thermal conductivity of frost. In

- International Symposium of Heat and Mass Transfer in Refrigeration Cryogenics*, Dubrovnik, 1986, pp. 285–302.
14. Whitaker, S., Simultaneous heat, mass and momentum transfer in porous media: a theory of drying. In *Advances in Heat Transfer*, ed. J. P. Hartnett and T. F. Irvine, Jr, Vol. 13. Academic Press, New York, 1977, pp. 119–203.
  15. Vafai, K. and Whitaker, S., Simultaneous heat and mass transfer accompanied by phase change in porous medium. *Journal of Heat Transfer*, 1986, **108**, 132–140.
  16. Patankar, S. V., *Numerical Heat Transfer and Fluid Flow*. McGraw-Hill, New York, 1980.
  17. Auracher, H., Heat transfer in frost and snow. In *Proceedings of the 6th International Heat Transfer Conference*, Toronto, Vol. 3. 1978, pp. 25–30.
  18. O'Neal, D. L. and Tree, D. R., A review of frost formation in simple geometries. *ASHRAE Transactions*, 1985, **91**, 267.
  19. Harraghy, P. G. and Barber J. M., Frost formation. In *Proceedings of the Institute of Refrigeration*, Vol. 83. 1987, pp. 13–27.
  20. Aoki, K., Katayama, K. and Hayashi, Y., A study on frost formation (the process of frost formation involving the phenomena of water permeation and freezing). *Bulletin of the JSME*, 1983, **26** (211–214), 87–93.
  21. Auracher, H., Water vapor diffusion and frost formation in capillaries, Annex 1972-1. In *Bulletin of the International Institute of Refrigeration*, Communications B1, B2, and E1, Freudenstadt, 1972, pp. 477–488.
  22. Yosida, Z., Physical studies on deposited snow, *Control Institute Low Temperatures Sciences, Hokkaido University, Series A*, 1955, **7**, 19–74.
  23. Sanders, C. T., Some physical aspects of frost formation on air cooled surfaces. IIR Congress of Refrigeration, Paper 3.15, 1971.
  24. Mao, Y., Besant, R. W. and Rezkallah, K. S., Measurement and correlations of frost properties with air flow over a flat plate. *ASHRAE Transactions*, 1992, **98** (Part 2), 65–78.
  25. Mao, Y., Besant R. W. and Falk, J., Measurement and correlations of frost properties with laminar airflow at room temperature over a flat plate. *ASHRAE Transactions*, 1993, **99** (Part 1), 739–745.
  26. Levenspiel, O., *Chemical Reaction Engineering*. John Wiley, New York, 1962.

#### APPENDIX: FROST THERMAL CONDUCTIVITY MODEL

The simple model of Auracher [13, 17], referred to as the combination model, has been selected to compute  $\lambda_c$ . The unit cell is considered to be divided into two parts with the same porosity connected in series, where the heat flux direction is, respectively, perpendicular and parallel to the ice crystals. The ratio of the perpendicularly oriented part being defined as the factor  $C_1$ , the whole unit cell conductivity is then obtained from

$$1/\lambda_c = C_1/\lambda_H + (1 - C_1)/\lambda_A \quad (\text{A1})$$

with  $\lambda_H$  and  $\lambda_A$  being the two weighted harmonic and arithmetic means of the ice and air conductivities:

$$\begin{cases} 1/\lambda_H = (1 - \varepsilon_x)/\lambda_i + \varepsilon_x/\lambda_a & (\text{perpendicular}) \\ \lambda_A = (1 - \varepsilon_x)\lambda_i + \varepsilon_x\lambda_a & (\text{parallel}) \end{cases} \quad (\text{A2})$$

with

$$C_1 = 0.42(0.1 + 0.995^u) \quad (\text{A3})$$

$$\begin{cases} \lambda_a = 630/T & 100 \leq T \leq 273 \\ \lambda_i \approx \lambda_a = -3.381 \times 10^{-8} T^2 + 9.814 \times 10^{-5} T \\ \quad - 1.308 \times 10^{-4} & 180 \leq T \leq 600. \end{cases} \quad (\text{A4})$$